HHS Public Access

Author manuscript

J Am Soc Mass Spectrom. Author manuscript; available in PMC 2019 November 01.

Published in final edited form as:

J Am Soc Mass Spectrom. 2018 November ; 29(11): 2115–2124. doi:10.1007/s13361-018-2026-7.

Operation and Performance of a Mass-Selective Cryogenic Linear Ion Trap

Larry F. Tesler, **Adam P. Cismesia**, **Matthew R. Bell**, **Laura S. Bailey**, and **Nicolas C. Polfer**

Department of Chemistry, University of Florida, P.O. Box 117200, Gainesville, FL 32611-7200, United States

Abstract

We report on the performance of a cryogenic 2D linear ion trap (cryoLIT) that is shown to be mass-selective in the temperature range of 17 – 295K. As the cryoLIT is cooled, the ejection voltages during the mass instability scan decrease, which results in an effective mass shift to lower *m/z* relative to room temperature. This is attributed to a decrease in trap radius caused by thermal contraction. Additionally, the cryoLIT generates reproducible mass spectra from day-to-day, and is capable of performing stored waveform inverse Fourier transform (SWIFT) mass isolation of fragile N_2-tagged ions for the purpose of background-free infrared dissociation spectroscopy.

Graphical Abstract

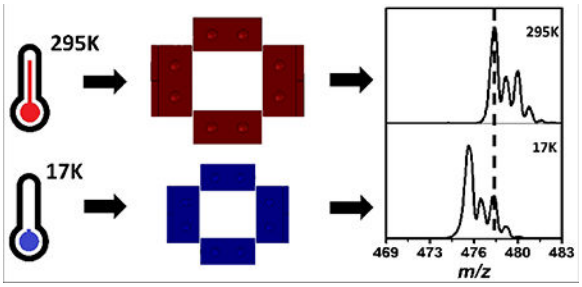

Keywords

infrared spectroscopy; tagging; cryogenic ion spectroscopy; cryogenics; linear ion trap

Introduction

The infrared spectra of mass-selected ions in a mass spectrometer can be recorded via “action” or “consequence” spectroscopy approaches, where, for instance, the ion is photodissociated with a tunable light source. The most readily implementable infrared ion spectroscopy technique is infrared multiple-photon dissociation (IRMPD) spectroscopy [1, 2], where typically room-temperature ions are subjected to intense radiation to cause absorption of several IR photons, leading to the cleavage of covalent bonds. IRMPD

Address reprint requests to Dr. Nicolas Polfer, Department of Chemistry, P.O. Box 117200, University of Florida, Gainesville, FL 32611-7200. polfer@chem.ufl.edu.

spectroscopy has been shown to be powerful in answering certain chemical questions about the structures of ions [3–5]. Nonetheless, the broader spectral features in IRMPD are an impediment to differentiating between closely-related molecules, especially when the number of putative structures is large. Higher resolution IR spectra can be generated at cryogenic temperatures [2, 6]; however, those approaches require custom instrumentation.

The first cryogenic IR "action" spectra of ions were recorded in supersonic expansions in the 1980's in the so-called *messenger* spectroscopy scheme [7]. In the expansion, ions are cooled to cryogenic temperatures, allowing inert gas atoms such as Ar (or *e.g.* Ne, He) to condense onto the ion. As the binding energy of this Van der Waals-tagged atom is lower than the energy of a single IR photon, resonant absorption of an IR photon leads to detachment of the Ar atom [8]. The basic premise of the messenger spectroscopy scheme is that detachment of the weakly-bound tag *reports* on photon absorption. Another assumption is that the weak binding of the tag only subtly affects the inherent absorption spectrum of the ion. In the 2000's, it was demonstrated that ions could also be cooled and tagged in cryogenic ion traps [9–11], either with He [12, 13], H_2 [14, 15], D_2 [16, 17], N_2 [18, 19]or Ne [20](so far), and that this approach could then be employed to measure cryogenic IR spectra of ions [12, 18, 20–26]. This major advance in principle allows the coupling of *any* ionization technique with cryogenic spectroscopic interrogation. In terms of biomolecular structure identification, the combination with electrospray ionization (ESI) especially stands out, and correspondingly there has been a surge in papers in recent years to demonstrate bioanalytical applications of IR ion spectroscopy [3, 18, 27–32], as well as cryogenic UV spectroscopy [33, 34].

As discussed in a recent *critical insight* article in this journal [35], cryogenic IR ion spectroscopy has the potential to become a gold standard technique for molecular identification in mass spectrometry, but still faces some significant challenges with respect to instrumentation and methodology to make the technique analytically useful. A key challenge in this respect is the low duty cycle of the experiment, as typically only one molecular species is probed at one light frequency at one time. In principle, the tagging scheme in cryogenic IR ion spectroscopy lends itself to a multiplexed approach, as the mass decrease/increase upon (de)tagging is completely predictable. Thus, the IR spectra of multiple tagged ions could be probed in parallel. As tagging efficiencies are generally low (i.e., few %), and ion intensities fluctuate from shot-to-shot, for signal-to-noise reasons it is not ideal to measure the depletion of the tagged ion as a function of IR frequency. Instead, by mass isolating the tagged ion, the appearance of the photodissociated untagged ion can be recorded in a background-free scheme. The measurement of the photodissociation yield compensates for random fluctuations in the tagged ion signal. To carry out such a background-free scheme on multiple tagged ions, it is critical that ions can be mass isolated *inside* a mass-selective cryogenic ion trap.

Cryogenic operation of Fourier transform ion cyclotron resonance (FTICR) traps has already been demonstrated [36, 37]; however, due to the image current detection scheme, these are generally less sensitive than rf traps [38]. Recently, we demonstrated IR spectroscopy results from the first mass-selective cryogenic 2D linear ion trap (cryoLIT) [39]. The rectilinear electrodes of this design combine simplicity in machining with the higher trapping

efficiencies and capacities of 2D linear ion traps vis-à-vis 3D ion traps [40–43]. The high dynamic range and low detection limits make 2D linear ion traps a compelling choice for ion spectroscopy, in order to enhance signal-to-noise in these ion intensity measurements. Here, we describe operation and performance of this custom LIT at both cryogenic and room temperatures.

Experimental

CryoLIT Design

The cryoLIT is set up as an extension to a previously described custom mass spectrometer [44]. Ions from a modified Electrospray Ionization (ESI) source (Analytica of Branford, Branford, CT) are directed to a quadrupole mass filter (QMF) (Ardara Technologies L.P., Ardara, PA), from where they can proceed to either a Quadrupole Ion Trap (QIT) (Jordan TOF Products, Grass Valley, CA), or a rectilinear accumulation trap. After accumulation in the rectilinear accumulation trap, ions are transferred to the cryoLIT.

Figure 1 shows a schematic of the cryoLIT, which is a rectilinear ion trap (RIT) inspired by the RIT designs of Ouyang/Cooks and Wang [41, 42]. The cryoLIT features an x-stretched geometry with an x to y electrode spacing ratio of 1.2. Specifically, the x-electrode half-spacing is 0.24”, and the y-electrode half-spacing is 0.20” (x/y = 1.2). The stretched geometry is advantageous for enhanced mass manipulation of ions, as it can partially compensate for the field imperfections due to the slits [41]. A dynode/electron multiplier detector (not shown in Figure 1) is placed in the line with the slits of the x electrodes. The slits are 0.04” wide. This value is a trade-off between adequate mass selectivity capabilities, good ejection efficiencies, and a sufficiently low gas conductance of the trap. The latter characteristic is important in order to achieve sufficient pressurization in the trap for cooling and Van der Waals-tagging of ions. The electrodes are held apart at a small distance of 0.02” to further reduce gas conductance. The electrodes are made from 17–4PH stainless steel to prevent possible warping of the trap during cooling. Sapphire spacers are employed to electrically insulate the electrodes, while at the same time providing thermal conductance.

A closed-cycle helium cryostat (AirProducts DE202, Allensville, PA, 1W cooling power at 15K) cools the cryoLIT; the cryoLIT is mounted on the copper coldfinger of the cryostat, which is mounted on top of a custom vacuum chamber. Several strategies are employed to reduce the thermal load on the cryoLIT. The DC electrode wires are wrapped around the coldfinger to achieve thermalization, a polished aluminum heatshield, held at 50K, encloses the trap to minimize blackbody heating, and the rf wires are (partially) thermalized *via* a heat sink on the heatshield. Two thermocouples (LakeShore DT-670 CU, Westerville, OH) monitor the temperature at the copper coldfinger and at one of the DC endplates. A heater cartridge, controlled by a cryogenic thermostat (LakeShore 335), regulates the coldfinger temperature. The buffer gas is introduced into the cryoLIT via a solenoid valve (Parker Series 99, Hollis, NH).

Electronics

A commercial Velos rf power supply (Thermo-Fisher, San Jose, CA) drives the cryoLIT at a fixed frequency of 1.108 MHz. The rf power supply is operated in a closed-loop mode to ensure that the rf amplitude does not fluctuate and broaden the mass spectra. A secondary transformer, inside the rf power supply, allows an auxiliary dipolar or "tickle" waveform to be coupled to the x-electrodes. The purpose of this tickle waveform is to radially excite ions in the x-plane to eject them from the trap either for mass selection or detection (*via* a dynode/electron multiplier). The tickle waveform is generated by either a PCI-5421 NI AWG for the Stored Waveform Inverse Fourier Transform (SWIFT), or a Stanford Research DS345 function generator for the fixed frequency dipolar waveform. The two function generators are coupled together by a BNC t-connector. The experimental timing is controlled via a combination of a Stanford Research DG645 delay generator and an ARM microcontroller (Teensy LC, Sherwood, OR), with a maximum timing jitter of +/− 250 ns.

Experimental Design

Figure 2 shows the key voltages on the rf electrodes during the experiment. After external ion injection, the ions are held at a constant main rf amplitude for the first 280 ms (e.g. 200 V_{0p}), and are allowed to collisionally cool with the injected helium gas pulse (5 ms duration at ~10–20 torr backing pressure). The pressure inside of the vacuum chamber holding the cryoLIT was monitored by a residual gas analyzer (Extorr, New Kensington, PA), and a sample pressure profile after the helium gas is injected is shown in Figure S1 in the Supplementary materials. At 300 ms, the main rf is scanned from 300 to 1500 V_{0p} over 200 ms, while simultaneously, a 369 kHz dipolar "tickle" excitation waveform is applied to the x-electrodes. The amplitude of this "tickle" waveform is also linearly increased (from 1 to 4 V_{0p}), to keep the amplitude low initially, and thus improve the resolution, while still being able to properly eject the higher *m/z* ions [40]. This frequency corresponds to a q-value of 0.784 and $\beta = 2/3$, and thus introduces a notch in the stability diagram. The purpose of this "tickle" waveform is twofold: (1) ions are selectively excited in the x plane (as opposed to the y-plane) to increase their detection efficiency through the slits in the x-electrodes to the dynode/electron multiplier detector; and (2) the lower critical q value results in an extension of the *m/z* range. The effective scan rate is 2000 Th s^{-1} from *m/z* 100 to 500.

In the N_2-tagging experiment, 5% nitrogen gas is added to the helium gas mixture, and the experiment is significantly shortened; the ions are only held at a constant rf amplitude for 100 ms, and the scan rate is increased to 4000 Th s^{-1} from m/z 200 to 600, to give an overall experiment time of 200 ms.

For mass isolation, a 5 ms dipolar SWIFT waveform [45] is applied to the x-electrodes to mass isolate the calibrant ions, while keeping the rf amplitude constant. Mass isolation windows are calculated using a custom Python program, which converts mass ranges into frequency ranges using the Mathieu equation. The frequency ranges are then converted using inverse Fourier transform procedure described by Chen *et. al* [45]. A frequency step size of 200 Hz is used to generate a 5 ms long SWIFT waveform. No windowing function is used as it does not significantly affect SWIFT performance [46].

Materials

Solutions containing a mixture of L-proline (M.W. = 115 Da), caffeine (M.W. = 195 Da), glutathione (M.W. = 307 Da), brucine (M.W. = 394 Da), and loperamide (M.W. = 476 Da) (Sigma Aldrich, St Louis, MO) are made at 10^{-5} M in a 70:30 methanol:water solution with 0.1% formic acid added into it to assist with ionization. The Tripeptide GYK (M.W. = 366 Da) is synthesized in-lab using standard FMOC procedures [47] on an Applied Biosystems SYNERGY model 432A peptide synthesizer. Electrospray Ionization (ESI) is used to protonate and nebulize the calibration solution. The solution flows to the ESI source at a flow rate of 2 μL min^{-1}.

Trajectory simulations

SIMION 8.0 (Scientific Instrument Services, Inc., Ringoes, NJ, USA) is used to simulate and characterize the cryoLIT at room temperature, using a grid size of 0.1 mm to calculate the electrode potentials. For the simulation, ions are initialized in a 3D Gaussian distribution at the center of the trap and are given a kinetic energy of 25 meV (room temperature kT) with a randomized orientation. Single ions with masses between 100 and 400 Th in steps of 10 Th are considered here. The ions are given 10 ms to equilibrate in the middle of the trap before the main rf is ramped from 300 to 1500 V_{0p}, with no dipolar excitation applied. Ions' time of flights are recorded when they exit the slit of the x-electrodes to determine the ejection rf amplitude for each *m/z* value. As some of the ions crash into the x and y electrodes during the simulation, the simulations are carried out repeatedly until there are at least 3 data points for each mass, to obtain a mean and standard deviation for the ejection rf amplitude.

Results and Discussion

Mass Calibration of the CryoLIT at Room Temperature

The relationship between the mass-to-charge ratio of the ejected ions, $\frac{m}{z}$(Th) and the applied main rf, V_{0p} (V), is given by Equation 1.

$$\frac{m}{z} = A_2 \frac{4eV_{0p}}{qN_a r_N^2 \Omega^2} \quad \text{Eq. 1}$$

where, A_2 is the quadrupole coefficient (unitless) in the multipole expansion of the potential inside the trap, representing the contribution of the quadrupolar field to the potential, e is the elementary charge (in C), N_a is Avogadro's number (mol^{-1}), q is the Mathieu parameter for the rf (unitless), Ω is the angular frequency of the rf (in rad s^{-1}), and r_N is the normalization radius (in m), which is taken to be as half of the y electrode spacing, 5.08×10^{-3} m or 0.20" (as this is the smaller dimension).

In an idealized quadrupolar field $A_2 = 1$ and can hence be neglected. Conversely, in stretched geometries, or rectilinear ion traps, it is expected that $A_2 < 1$. There are various approaches to estimate A_2, either via simulations or experiment. Figure 3 shows the results

from a numerical SIMION simulation, where ions in a *m/z* range 100–400 are ejected through the x-electrodes via a mass instability scan. A best fit line of *m/z* vs. ejection rf amplitude $V_{0\text{-}p}$ yields a slope of 0.2985. By dividing this slope by $\frac{4e}{qN_a r_N^2 \Omega^2}$ (where q = 0.908), A_2 is found to be equal to 0.884. An alternative approach to estimate A_2 theoretically involves fitting the SIMION-obtained potentials inside the trap to a multipole expansion equation [48, 49] (see section 2 in the Supplementary materials for a detailed description of this method), and with this method we predict A_2 to be 0.866. Experimentally, A_2 is estimated to be 0.867, based on a mass instability scan obtained at room temperature. Note that for the experimental result, the same equation as above is used but, as a dipolar tickle excitation waveform is employed, q is changed to 0.784. These experimental results are shown later in the manuscript (i.e., 295K data in Fig 5). It appears therefore that the multipole expansion equation yields the most accurate determination of A_2, even if there are some caveats here in terms of grid size and boundaries.

Table 1 contains a summary of the A_2 values determined for the cryoLIT, along with the simulation-derived A_2 values for the rectilinear ion traps designed by Ouyang/Cooks and Wang [41, 42]. The cryoLIT features a larger A_2, and thus a greater quadrupolar field, than these other two traps, which may be a result of the smaller electrode gaps. In principle, a greater A_2 suggests a better approximation to an ideal quadrupolar ion trap; however, the higher order fields (*i.e.* octupolar, dodecapolar) also play an important part in improving the mass resolution during a mass instability scan by compensating for the reduction in electric field caused by the trap slits [41].

Modeling the Thermal Contraction of the CryoLIT

As the temperature of the cryoLIT is brought down to cryogenic levels, the trap is expected to experience thermal contraction, which will naturally affect its performance. The cryoLIT can be cooled down to 17K, and according to the linear thermal expansion data for 17–4PH stainless steel, the electrodes are expected to contract by 0.202% [50].If the rf electrodes did not move, the trap radius should increase as the rf electrodes contract, but since the rf electrodes are held in position by the DC endcaps, which are larger than the rf electrodes, the overall trap radius should decrease. This is illustrated in Figure S3. By taking both the shrinking of the rf electrodes and DC endcaps into account, the trap radius should decrease by 0.200% in the y-direction and 0.200% in the x-direction (see Eq. S3 and S4 in the Supplementary materials for a detailed calculation of these values). Given that the rf voltage at which an ion of a particular mass ejects from the cryoLIT is dependent on the trap radius (Equation 1), we should expect that if the trap radius does in fact decrease, with all other parameters held constant, the observed mass spectra at cryogenic temperatures should be shifted to lower masses (with respect to calibrated room-temperature mass spectra).

Effect of Cooldown on Mass Spectra

Figure 4 compares the mass spectra recorded at room temperature and cryogenic temperature (17K). The zoomed-in plots highlight that at cryogenic temperatures, the apparent *m/z* of the ions are lower with respect to the room temperature calibration. This suggests that the ejection voltages for each ion are lower at cryogenic temperatures. A slight

reduction in resolving power is observed when cooling the trap from 295K to 17K. Figure 5 shows the equivalent data in Figure 4 as a calibration slope of actual *m/z vs.* measured rf ejection voltage, based on a linear regression fit. For the cryogenic temperature mass spectrum, the slope is 0.32% higher than the room-temperature slope, so correspondingly, the ejection voltages are lower. If we look at Equation 1, we can see that the change in slope must be caused by a change in one of the parameters. Based on the thermal contraction of the trap, one expects a decrease in trap radius, and consequently an increase in the calibration slope.

To systematically determine how the temperature affects the calibration slope, the mass spectra of the calibration mixture are collected at a series of temperatures. In Figure 5, the relative differences between the cryogenic and room temperature calibration slopes, $\frac{k_T - k_{295K}}{k_T}$ are plotted as function of temperature, and this is contrasted to the thermal contraction of the radius (as calculated in Section 2 in Supplementary Materials) multiplied by 2. This relative difference expression is used, as it can be converted and simplified to an expression containing the thermal contraction, showing that the relative difference in calibration slope is equal to *twice* the thermal contraction (Equation 2).

$$\frac{k_T - k_{295K}}{k_T} = \frac{\frac{1}{(r-\Delta r)^2} - \frac{1}{r^2}}{\frac{1}{(r-\Delta r)^2}} = 1 - \frac{(r-\Delta r)^2}{r^2} \approx 1 - \frac{r^2 - 2r\Delta r}{r^2} = \frac{2\Delta r}{r} \quad \text{Eq. 2}$$

Using the thermal contraction data for 17–4PH stainless steel [50], the cryoLIT trap radius should shrink by 0.200% in the x- and y-direction, and therefore, the relative difference in calibration slope should be equal to −0.400%, which is a reasonable match with the maximum change in slope of −0.34%. Furthermore, there is no measurable mass shift below 50K, which mirrors the flattening of the thermal contraction curve in that temperature range. While the general trend of the change in slopes matches the change in trap radius, the slope differences are systematically lower; this could potentially be a change in A_2 that occurs during cooling.

Interday Repeatability

After operating the cryoLIT (typically 8 hours), it is warmed back to room temperature to get rid of adsorbed water and gasses. Repeated cooling and warming may result in accumulated geometrical changes that adversely affect the calibration of the mass spectra. To determine how repeatable the mass spectra are from day to day, the mass spectra of the calibration. Therefore, even with repeated temperature cycling of the cryoLIT, the mass spectra are highly reproduciblemixture are collected over several days, bringing the trap repeatedly back to room temperature at the end of each experiment. The average deviation of the masses over these runs at 17K is 0.04 ± 0.03 *m/z*, significantly less than the mass resolution of the cryoLIT.

SWIFT Mass Isolation

To perform infrared photodissociation (IRPD), the tagged analyte ions need to be isolated by ejecting the remainder of the untagged species. For a single untagged-tagged pair, this can be achieved by increasing the rf amplitude to the point where the untagged ion m/z is above the stability diagram critical value q=0.908. However, when attempting to acquire the IRPD spectra of several tagged ions simultaneously, i.e., multiplexing, this method is insufficient. SWIFT isolation waveforms can be used to isolate multiple tagged ions by using a broadband signal, with notches in the frequency spectrum for each isolated mass. Figure 7 shows caffeine (*m/z* 195) and brucine (*m/z* 395) being isolated from the rest of the calibration mixture. There is no significant loss of intensity for a 5 ms 350 mV_{0p} SWIFT waveform with ±5 *m/z* notches, and the mass spectrum is generally low in noise; however, there is a peak at *m/z* 387 that is not removed, as it falls inside the mass isolation window.

Figure 8 shows an attempt to N_2-tag GYK (tripeptide) ions inside the cryoLIT. Setting the cryoLIT DC endplates to 23K and adding a small amount (~5%) of nitrogen in the helium gas pulse mixture results in peaks appearing at *m/z* 395 (367 + 28) and *m/z* 423 (367 + 2 * 28). This corresponds to singly- and doubly-tagged GYK, respectively. Interestingly, other publications report that N_2 –tagging can occur at temperatures near liquid N_2 (60–70K)[18], but we observe little to no tagging of GYK above 30K. To demonstrate that N_2-tagged ions can be isolated inside of the cryoLIT, an 8 ms SWIFT waveform with a ± 10 m/z notch over the singly N_2-tagged is applied (Figure 8B). Note that after SWIFT isolation there is a negligible amount of the untagged ion remaining, and it is on the same order as the doubly-tagged signal. This suggests that there is a very small amount of dissociation of tag during the application of the SWIFT and mass scan; given that the binding energy of a van der Waals tag is on the order of 10 meV (600–970 cm^{-1}) [14, 19, 51], it is remarkable that the background fragmentation is so low. With the singly-tagged GYK ion isolated, the infrared predissociation (IRPD) spectrum can be acquired by irradiating the trapped ions with our tunable IR laser, and this IRPD spectrum is shown in Figure 8C.

Conclusions

In summary, we have demonstrated that the cryoLIT is mass-selective in the temperature range between 17 and 295K, without any significant loss in performance. Mass shifts upon cooling can be rationalized by a thermal contraction of the trap. These shifts are reproducible on a day-to-day basis, and they can be corrected for by a simple calibration. Multiple analyte ions can be mass isolated via a SWIFT waveform, and this is a basic prerequisite for multiplexed IR spectroscopy on multiple tagged analytes, which will significantly improve throughput. When mass isolating tagged ions (*e.g.* GYK●N_2), extra consideration must be taken when generating a SWIFT waveform. Since the tagged ions are fragile, wider notches (> ±10 *m/z*) must be employed to prevent activating the tagged ions. This also rationalizes the choice of the tag as N_2, which shifts the mass by 28 amu, as opposed to H_2 or D_2.

With a mass range of 100–700 *m/z* (the upper mass limit is not shown here), the cryoLIT is suitable for the study of small molecules such as metabolites. Future work will focus on addressing current limitations. Our current experiment is rather long (200–500 ms), which

does not match the output pulses from the optical parametric oscillator (OPO) operated at 10 Hz.

The experiment will need to be shortened by 2–5 times to achieve a 100% duty cycle. Additionally, this stainless steel cryoLIT can only reach 17K, which is too warm to perform tagging with lighter gases (*e.g.* H_2/D_2, Ne). Moving to a copper trap could address this issue [12, 35, 52].

Supplementary Material

Refer to Web version on PubMed Central for supplementary material.

Acknowledgements

The project was financially supported by the United States National Science Foundation (NSF) under grant number CHE-1403262 and the United States National Institutes of Health (NIH) under grant number R01GM110077. Todd Prox and Brian Smith in our machine shop are gratefully acknowledged for constructing the *cryo*LIT and a number of custom parts of our set-up. Stanley Pych in our electronics shop is acknowledged for his help with electronics circuits. Dr. Philip Remes and Dr. Jae Schwartz from Thermo-Fisher are thanked for providing a Thermo rf power supply to enable these experiments.

References

1. Polfer NC, Oomens J: Vibrational spectroscopy of bare and solvated ionic complexes of biological relevance. Mass Spectrom. Rev 28, 468–494 (2009). doi:10.1002/mas.20215 [PubMed: 19241457]
2. Fridgen TD: Infrared consequence spectroscopy of gaseous protonated and metal ion cationized complexes. Mass Spectrom. Rev 28, 586–607 (2009). doi:10.1002/mas.20224 [PubMed: 19343731]
3. Hernandez O, Isenberg S, Steinmetz V, Glish GL, Maitre P: Probing Mobility-Selected Saccharide Isomers: Selective Ion–Molecule Reactions and Wavelength-Specific IR Activation. J. Phys. Chem. A 119, 6057–6064 (2015). doi:10.1021/jp511975f [PubMed: 25827317]
4. Lanucara F, Chiavarino B, Scuderi D, Maitre P, Fornarini S, Crestoni ME: Kinetic control in the CID-induced elimination of H3PO4 from phosphorylated serine probed using IRMPD spectroscopy. Chem. Commun 50, 3845–3848 (2014). doi:10.1039/C4CC00877D
5. Prell JS, Flick TG, Oomens J, Berden G, Williams ER: Coordination of Trivalent Metal Cations to Peptides: Results from IRMPD Spectroscopy and Theory. J. Phys. Chem. A 114, 854–860 (2010). doi:10.1021/jp909366a [PubMed: 19950916]
6. Rizzo TR, Stearns JA, Boyarkin OV: Spectroscopic studies of cold, gas-phase biomolecular ions. Int. Rev. Phys. Chem 28, 481–515 (2009). doi:10.1080/01442350903069931
7. Okumura M, Yeh LI, Myers JD, Lee YT: Infrared spectra of the cluster ions H7O+3H2 and H9O +4H2. J. Chem. Phys 85, 2328–2329 (1986). doi:10.1063/1.451079
8. Robertson WH, Kelley JA, Johnson MA: A pulsed supersonic entrainment reactor for the rational preparation of cold ionic complexes. Rev. Sci. Instrum 71, 4431–4434 (2000). doi: 10.1063/1.1326931
9. Wang X-B, Wang L-S: Development of a low-temperature photoelectron spectroscopy instrument using an electrospray ion source and a cryogenically controlled ion trap. Rev. Sci. Instrum 79, 073108 (2008). doi:10.1063/1.2957610 [PubMed: 18681692]
10. Gunther A, Nieto P, Muller D, Sheldrick A, Gerlich D, Dopfer O: BerlinTrap: A new cryogenic 22-pole ion trap spectrometer. J. Mol. Spectrosc 332, 8–15 (2017). doi:10.1016/j.jms.2016.08.017
11. Fanghänel S, Asvany O, Schlemmer S: Optimization of RF multipole ion trap geometries. J. Mol. Spectrosc 332, 124–133 (2017). doi:10.1016/j.jms.2016.12.003
12. Roithová J, Gray A, Andris E, Jašík J, Gerlich D: Helium Tagging Infrared Photodissociation Spectroscopy of Reactive Ions. Acc. Chem. Res 49, 223–230 (2016). doi:10.1021/acs.accounts. 5b00489 [PubMed: 26821086]

13. Asvany O, Brünken S, Kluge L, Schlemmer S: COLTRAP: a 22-pole ion trapping machine for spectroscopy at 4 K. Appl. Phys. B 114, 203–211 (2014). doi:10.1007/s00340-013-5684-y
14. Kamrath MZ, Relph RA, Guasco TL, Leavitt CM, Johnson MA: Vibrational predissociation spectroscopy of the H2-tagged mono- and dicarboxylate anions of dodecanedioic acid. Int. J. Mass Spectrom 300, 91–98 (2011). doi:10.1016/j.ijms.2010.10.021
15. Masson A, Kamrath MZ, Perez MAS, Glover MS, Rothlisberger U, Clemmer DE, Rizzo TR: Infrared Spectroscopy of Mobility-Selected H+-Gly-Pro-Gly-Gly (GPGG). J. Am. Soc. Mass Spectrom 26, 1444–1454 (2015). doi:10.1007/s13361-015-1172-4 [PubMed: 26091889]
16. Leavitt CM, Wolk AB, Fournier JA, Kamrath MZ, Garand E, Van Stipdonk MJ, Johnson MA: Isomer-Specific IR–IR Double Resonance Spectroscopy of D2-Tagged Protonated Dipeptides Prepared in a Cryogenic Ion Trap. J. Phys. Chem. Lett 3, 1099–1105 (2012). doi:10.1021/jz3003074 [PubMed: 26288043]
17. Marsh BM, Voss JM, Garand E: A dual cryogenic ion trap spectrometer for the formation and characterization of solvated ionic clusters. J. Chem. Phys 143, 204201 (2015). doi:10.1063/1.4936360 [PubMed: 26627952]
18. Masellis C, Khanal N, Kamrath MZ, Clemmer DE, Rizzo TR: Cryogenic Vibrational Spectroscopy Provides Unique Fingerprints for Glycan Identification. J. Am. Soc. Mass Spectrom 28, 2217–2222 (2017). doi:10.1007/s13361-017-1728-6 [PubMed: 28643189]
19. Andrei H-S, Solcà N, Dopfer O: Interaction of Ionic Biomolecular Building Blocks with Nonpolar Solvents: Acidity of the Imidazole Cation (Im+) Probed by IR Spectra of Im+−Ln Complexes (L = Ar, N2; n ≤ 3). J. Phys. Chem. A 109, 3598–3607 (2005). doi:10.1021/jp0441487 [PubMed: 16839026]
20. Jašík J, Roithová J: Infrared spectroscopy of CHCl2+ molecular dications. Int. J. Mass Spectrom 377, 109–115 (2015). doi:10.1016/j.ijms.2014.07.001
21. Kamrath MZ, Garand E, Jordan PA, Leavitt CM, Wolk AB, Van Stipdonk MJ, Miller SJ, Johnson MA: Vibrational Characterization of Simple Peptides Using Cryogenic Infrared Photodissociation of H2-Tagged, Mass-Selected Ions. J. Am. Chem. Soc 133, 6440–6448 (2011). doi:10.1021/ja200849g [PubMed: 21449591]
22. Goebbert DJ, Wende T, Bergmann R, Meijer G, Asmis KR: Messenger-Tagging Electrosprayed Ions: Vibrational Spectroscopy of Suberate Dianions. J. Phys. Chem. A 113, 5874–5880 (2009). doi:10.1021/jp809390x [PubMed: 19391586]
23. Dillinger S, Klein MP, Steiner A, McDonald DC, Duncan MA, Kappes MM, Niedner-Schatteburg G: Cryo IR Spectroscopy of N2 and H2 on Ru8+: The Effect of N2 on the H-Migration. J. Phys. Chem. Lett 9, 914–918 (2018). doi:10.1021/acs.jpclett.8b00093 [PubMed: 29406747]
24. Duffy EM, Marsh BM, Voss JM, Garand E: Characterization of the Oxygen Binding Motif in a Ruthenium Water Oxidation Catalyst by Vibrational Spectroscopy. Angew. Chem. Int. Ed Engl 55, 4079–4082 (2016). doi:10.1002/anie.201600350 [PubMed: 26890565]
25. Mohrbach J, Lang J, Dillinger S, Prosenc M, Braunstein P, Niedner-Schatteburg G: Vibrational fingerprints of a tetranuclear cobalt carbonyl cluster within a cryo tandem ion trap. J. Mol. Spectrosc 332, 103–108 (2017). doi:10.1016/j.jms.2016.11.008
26. Thompson MC, Ramsay J, Weber JM: Solvent-Driven Reductive Activation of CO2 by Bismuth: Switching from Metalloformate Complexes to Oxalate Products. Angew. Chem. Int. Ed 55, 15171–15174 (2016). doi:10.1002/anie.201607445
27. Martens J, Koppen V, Berden G, Cuyckens F, Oomens J: Combined Liquid Chromatography-Infrared Ion Spectroscopy for Identification of Regioisomeric Drug Metabolites. Anal. Chem 89, 4359–4362 (2017). doi:10.1021/acs.analchem.7b00577 [PubMed: 28368097]
28. Gorlova O, Colvin SM, Brathwaite A, Menges FS, Craig SM, Miller SJ, Johnson MA: Identification and Partial Structural Characterization of Mass Isolated Valsartan and Its Metabolite with Messenger Tagging Vibrational Spectroscopy. J. Am. Soc. Mass Spectrom 28, 2414–2422 (2017). doi:10.1007/s13361-017-1767-z [PubMed: 28801884]
29. Patrick AL, Stedwell CN, Polfer NC: Differentiating Sulfopeptide and Phosphopeptide Ions via Resonant Infrared Photodissociation. Anal. Chem 86, 5547–5552 (2014). doi:10.1021/ac500992f [PubMed: 24823797]

30. Schindler B, Barnes L, Renois G, Gray C, Chambert S, Fort S, Flitsch S, Loison C, Allouche A-R, Compagnon I: Anomeric memory of the glycosidic bond upon fragmentation and its consequences for carbohydrate sequencing. Nat. Commun 8, 973 (2017). doi:10.1038/s41467-017-01179-y [PubMed: 29042546]

31. Cismesia AP, Bell MR, Tesler LF, Alves M, Polfer NC: Infrared ion spectroscopy: an analytical tool for the study of metabolites. Analyst. 143, 1615–1623 (2018). doi:10.1039/C8AN00087E [PubMed: 29497730]

32. Seo J, Hoffmann W, Warnke S, Huang X, Gewinner S, Schöllkopf W, Bowers MT, Helden G von, Pagel, K.: An infrared spectroscopy approach to follow β-sheet formation in peptide amyloid assemblies. Nat. Chem 9, 39–44 (2017). doi:10.1038/nchem.2615 [PubMed: 27995915]

33. Kopysov V, Makarov A, Boyarkin OV: Identification of Isomeric Ephedrines by Cold Ion UV Spectroscopy: Toward Practical Implementation. Anal. Chem 89, 544–547 (2017). doi:10.1021/acs.analchem.6b04182 [PubMed: 27992166]

34. Burke NL, Redwine JG, Dean JC, McLuckey SA, Zwier TS: UV and IR spectroscopy of cold protonated leucine enkephalin. Int. J. Mass Spectrom 378, 196–205 (2015). doi:10.1016/j.ijms.2014.08.012

35. Cismesia AP, Bailey LS, Bell MR, Tesler LF, Polfer NC: Making Mass Spectrometry See the Light: The Promises and Challenges of Cryogenic Infrared Ion Spectroscopy as a Bioanalytical Technique. J. Am. Soc. Mass Spectrom 27, 757–766 (2016). doi:10.1007/s13361-016-1366-4 [PubMed: 26975370]

36. Meyer J, Tombers M, van Wüllen C, Niedner-Schatteburg G, Peredkov S, Eberhardt W, Neeb M, Palutke S, Martins M, Wurth W: The spin and orbital contributions to the total magnetic moments of free Fe, Co, and Ni clusters. J. Chem. Phys 143, 104302 (2015). doi:10.1063/1.4929482 [PubMed: 26374030]

37. Wong RL, Paech K, Williams ER: Blackbody infrared radiative dissociation at low temperature: hydration of X2+(H2O)n, for X = Mg, Ca. Int. J. Mass Spectrom 232, 59–66 (2004). doi:10.1016/j.ijms.2003.11.008

38. Marshall Alan G, Hendrickson Christopher L, Jackson George S: Fourier transform ion cyclotron resonance mass spectrometry: A primer. Mass Spectrom. Rev 17, 1–35 (1998). doi:10.1002/(SICI)1098–2787(1998)17:1<1::AID-MAS1>3.0.CO;2-K [PubMed: 9768511]

39. Cismesia AP, Tesler LF, Bell MR, Bailey LS, Polfer NC: Infrared ion spectroscopy inside a mass-selective cryogenic 2D linear ion trap. J. Mass Spectrom 52, 720–727 (2017). doi:10.1002/jms.3975 [PubMed: 28750482]

40. Schwartz JC, Senko MW, Syka JEP: A two-dimensional quadrupole ion trap mass spectrometer. J. Am. Soc. Mass Spectrom 13, 659–669 (2002). doi:10.1016/S1044-0305(02)00384-7 [PubMed: 12056566]

41. Ouyang Z, Wu G, Song Y, Li H, Plass WR, Cooks RG: Rectilinear Ion Trap: Concepts, Calculations, and Analytical Performance of a New Mass Analyzer. Anal. Chem 76, 4595–4605 (2004). doi:10.1021/ac049420n [PubMed: 15307768]

42. Wang L, Xu FX, Dai XH, Fang X, Ding CF: Development and Investigation of a Mesh-Electrode Linear Ion Trap (ME-LIT) Mass Analyzer. J. Am. Soc. Mass Spectrom 25, 548–555 (2014). doi:10.1007/s13361-013-0803-x [PubMed: 24435796]

43. Quarmby ST, Yost RA: Fundamental studies of ion injection and trapping of electrosprayed ions on a quadrupole ion trap22Dedicated to J.F.J. Todd and R.E. March in recognition of their original contributions to quadrupole ion trap mass spectrometry. Int. J. Mass Spectrom 190–191, 81–102 (1999). doi:10.1016/S1387-3806(98)14268-9

44. Gulyuz K, Stedwell CN, Wang D, Polfer NC: Hybrid quadrupole mass filter/quadrupole ion trap/time-of-flight-mass spectrometer for infrared multiple photon dissociation spectroscopy of mass-selected ions. Rev. Sci. Instrum 82, 054101 (2011). doi:10.1063/1.3585982 [PubMed: 21639521]

45. Chen L, Wang TC, Ricca TL, Marshall AG: Phase-modulated stored waveform inverse Fourier transform excitation for trapped ion mass spectrometry. Anal. Chem 59, 449–54 (1987) [PubMed: 3565762]

46. Soni MH, Cooks RG: Selective Injection and Isolation of Ions in Quadrupole Ion Trap Mass Spectrometry Using Notched Waveforms Created Using the Inverse Fourier Transform. Anal. Chem 66, 2488–2496 (1994). doi:10.1021/ac00087a013

47. Albericio F, Kates S: Solid-Phase Synthesis: A Practical Guide. CRC Press (2000)

48. Barlow SE, Taylor AE, Swanson K: Determination of analytic potentials from finite element computations. Int. J. Mass Spectrom. Ion Process 207, 19–29 (2001). doi:10.1016/S1387-3806(00)00452-8

49. Krishnaveni A, Verma NK, Menon AG, Mohanty AK: Numerical observation of preferred directionality in ion ejection from stretched rectilinear ion traps. Int. J. Mass Spectrom. Ion Process 275, 11–20 (2008). doi:10.1016/j.ijms.2008.05.011

50. Schwartzberg FR, Osgood SH, Keys RD, Kiefer TF: Cryogenic Materials Data Handbook Defense Technical Information Center, Ft. Belvoir (1964)

51. Fournier JA, Wolk AB, Johnson MA: Integration of Cryogenic Ion Vibrational Predissociation Spectroscopy with a Mass Spectrometric Interface to an Electrochemical Cell. Anal. Chem 85, 7339–7344 (2013). doi:10.1021/ac401228y [PubMed: 23767985]

52. Ishiuchi S, Wako H, Kato D, Fujii M: High-cooling-efficiency cryogenic quadrupole ion trap and UV-UV hole burning spectroscopy of protonated tyrosine. J. Mol. Spectrosc 332, 45–51 (2017). doi:10.1016/j.jms.2016.10.011

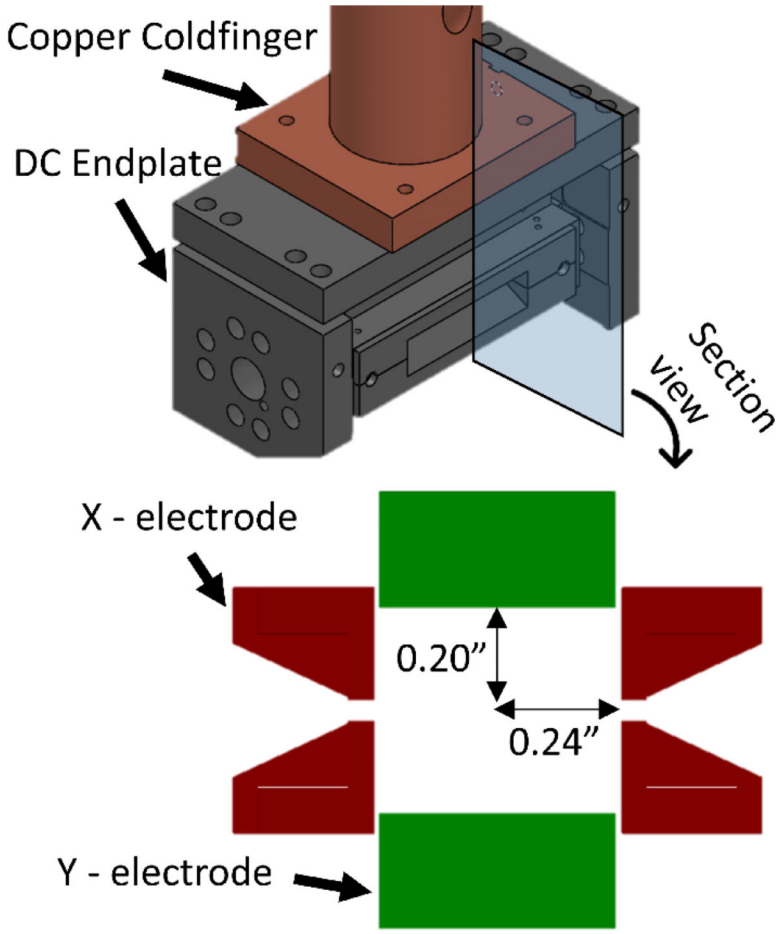

Figure 1.
CAD model of the cryoLIT assembly with a cross-sectional view illustrating the x and y-electrodes.

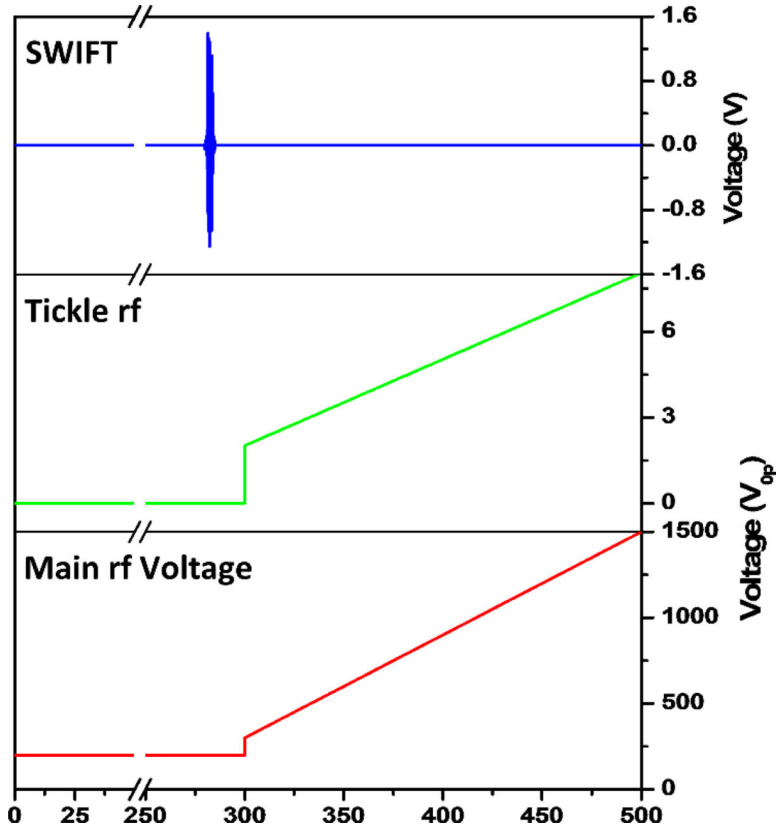

Figure 2.

Experimental scheme for the mass instability scans. A SWIFT waveform is applied 20 ms before the scan, for 5 ms. During the mass scan, both the resonant auxiliary frequency and the main rf amplitude are ramped up.

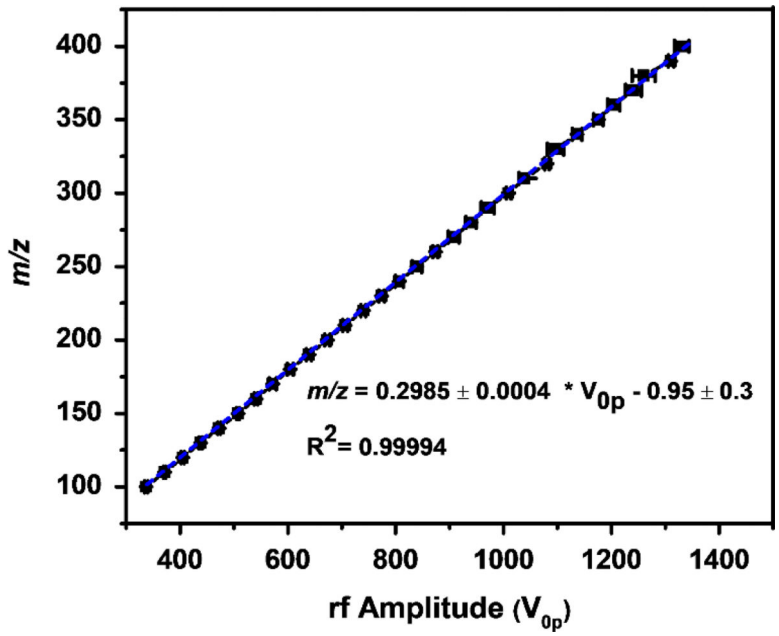

Figure 3.

SIMION-simulated mass calibration curve, the mean rf amplitude and standard deviation needed to eject a particular m/z, from the cryoLIT, from triplicate measurements. A_2 is calculated from the linear fit slope.

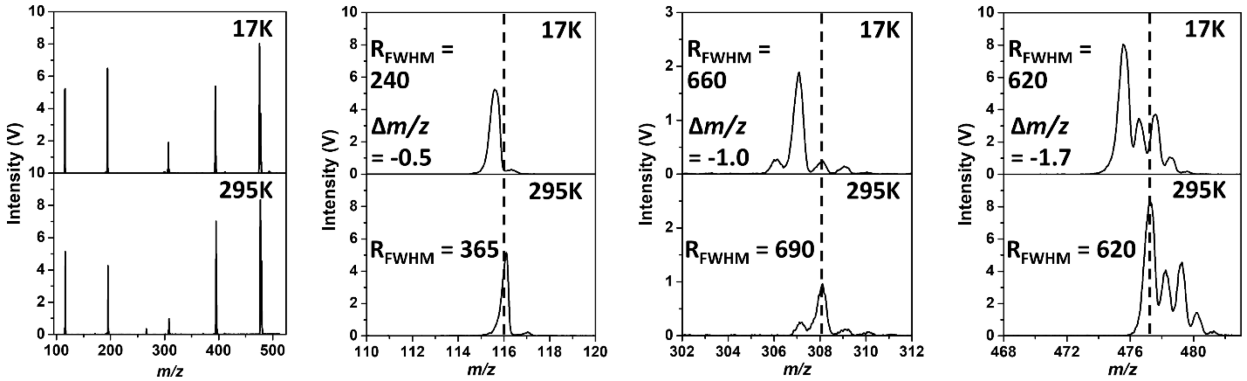

Figure 4.

Comparison between the room temperature (295K) (bottom) and cryogenic (top) mass spectra. The mass shift is more pronounced at higher masses as shown in the zoomed portions of the mass spectra (right).

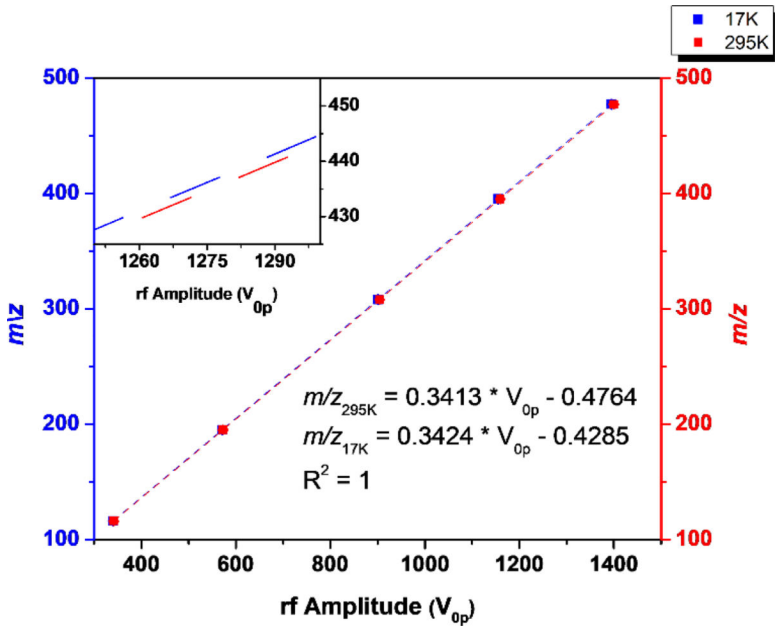

Figure 5.

The mass calibration lines for room (red) and cryogenic temperature (blue) mass instability scan. The cryogenic temperature scan features a higher slope which corresponds to lower ejection voltages. The inset shows a blown-up view of the 1250–1300 V region to illustrate the difference in slope.

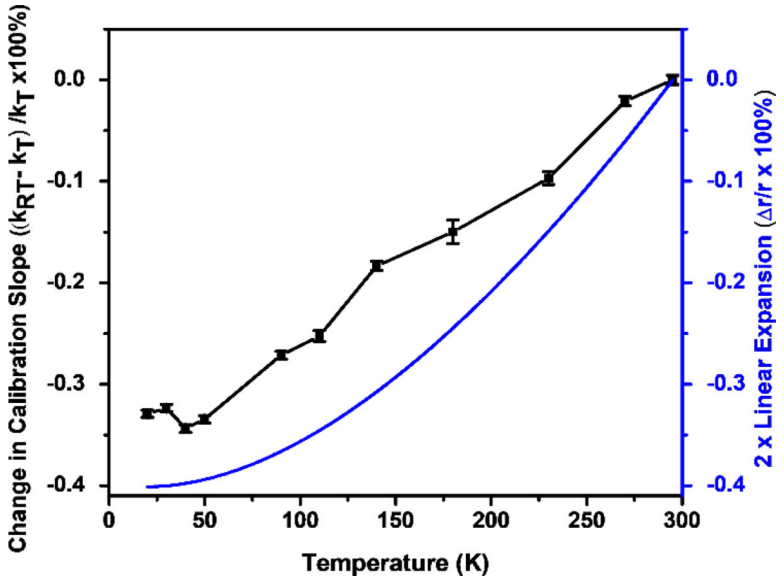

Figure 6.

The relative difference of calibration slopes relative to room temperature is plotted as function of temperature (black) alongside with the thermal contraction relative to room temperature (blue)[50], multiplied by 2.

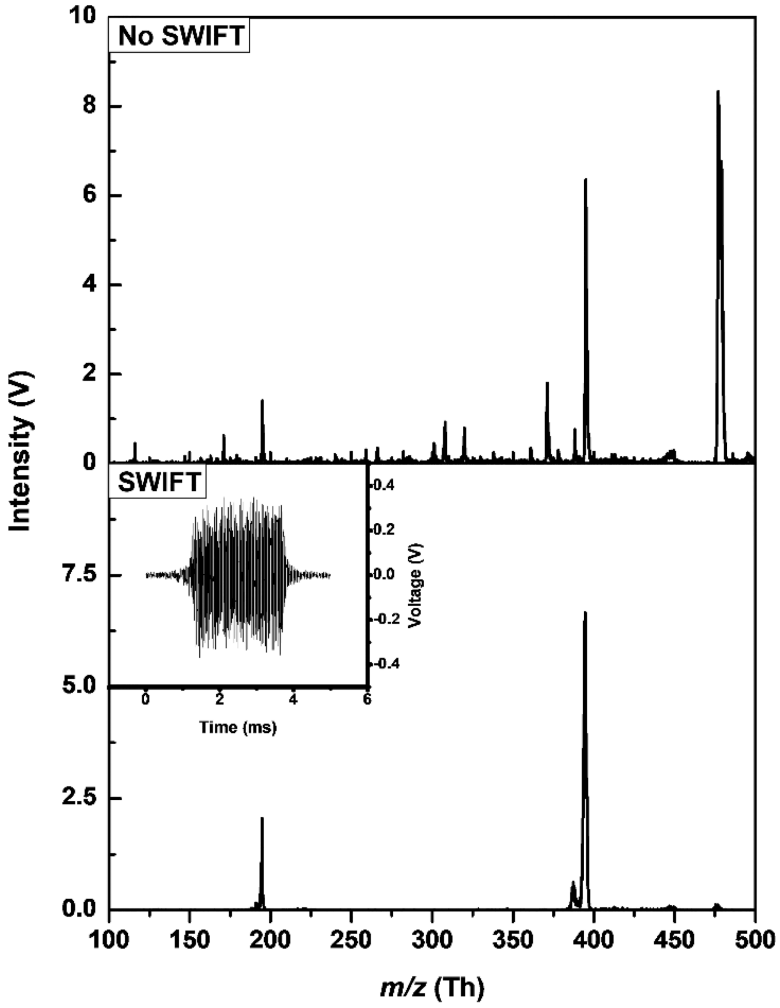

Figure 7.

SWIFT isolation of caffeine (m/z 195) and brucine (m/z 395) from a mixture of proline, caffeine, glutathione, brucine, and loperamide, performed at 17K. The SWIFT waveform is shown on the bottom left inset.

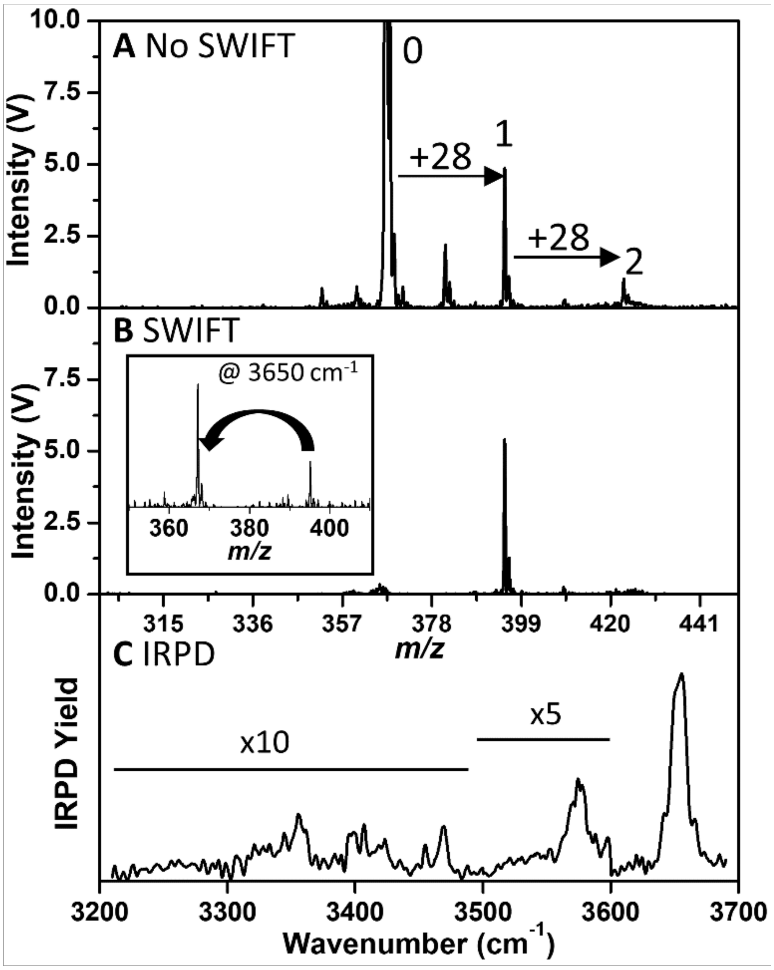

Figure 8.

(A) Mass Spectrum of GYK and its singly (1) and doubly (2) N_2-tagged ions. (B) SWIFT-isolated mass spectrum of the singly N_2-tagged GYK ion. The inset shows the mass spectrum after the loss of the dinitrogen tag upon absorption of an IR photon at 3650 cm^{-1}. (C) Infrared predissociation spectrum of the singly-tagged GYK ion.

Table 1.

A_2 values obtained for the cryoLIT using several different methods, along with reported A_2 values for the Cooks' RIT and Wang's Mesh-LIT.

Simulated Mass Instability	Multipole Expansion Fit	Experimental Mass Instability	Ouyang & Cooks RIT [41]	Wang Mesh-LIT [42]
0.884	0.866	0.867	0.633	0.806